New type of pore-snap-off and displacement correlations in imbibition

Journal of Colloid and Interface Science 609 (2022) 384–392

Contents lists available at ScienceDirect

Journal of Colloid and Interface Science

journal homepage: www.elsevier.com/locate/jcis

New type of pore-snap-off and displacement correlations in imbibition

Kamaljit Singh [a,b,*], Tom Bultreys [c,d], Ali Q. Raeini [e], Mosayeb Shams [e], Martin J. Blunt [b]

[a] Institute of GeoEnergy Engineering, Heriot-Watt University, EH14 4AS Edinburgh, UK
[b] Qatar Carbonates and Carbon Storage Research Centre, Department of Earth Science and Engineering, Imperial College London, SW7 2AZ London, UK
[c] Department of Geology, Pore-Scale Processes in Geomaterials Research (PProGRess), Ghent University, Krijgslaan 281/S8, B-9000 Ghent, Belgium
[d] Centre for X-ray Tomography (UGCT), Ghent University, Proeftuinstraat 86, B-9000 Ghent, Belgium
[e] Department of Earth Science and Engineering, Imperial College London, SW7 2AZ London, UK

GRAPHICAL ABSTRACT

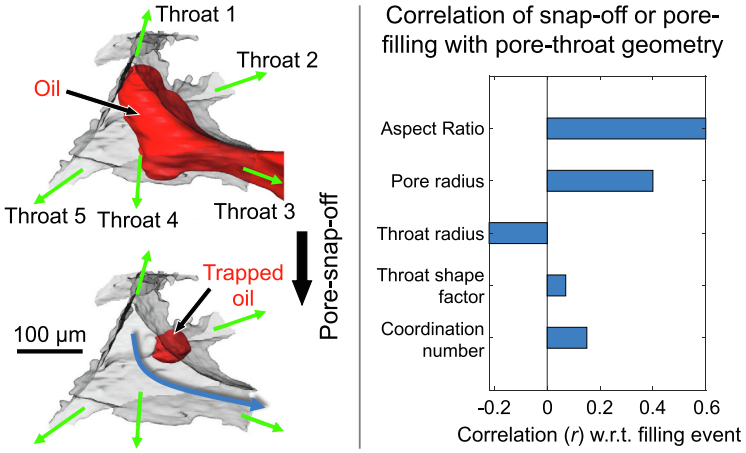

ARTICLE INFO

Article history:
Received 25 June 2021
Revised 18 November 2021
Accepted 19 November 2021
Available online 27 November 2021

Keywords:
Imbibition
snap-off
pore-filling
multiphase flow
porous media
4D X-ray imaging

ABSTRACT

Hypothesis: Imbibition of a fluid into a porous material involves the invasion of a wetting fluid in the pore space through piston-like displacement, film and corner flow, snap-off and pore bypassing. These processes have been studied extensively in two-dimensional (2D) porous systems; however, their relevance to three-dimensional (3D) natural porous media is poorly understood. Here, we investigate these pore-scale processes in a natural rock sample using time-resolved 3D (i.e., four-dimensional or 4D) X-ray imaging.
Experiments: We performed a capillary-controlled drainage-imbibition experiment on an initially brine-saturated carbonate rock sample. The sample was imaged continuously during imbibition using 4D X-ray imaging to visualize and analyze fluid displacement and snap-off processes at the pore-scale.
Findings: We discover a new type of snap-off that occurs in pores, resulting in the entrapment of a small portion of the non-wetting phase in pore corners. This contrasts with previously-observed snap-off in throats which traps the non-wetting phase in pore centers. We relate the new type of pore-snap-off to the pinning of fluid–fluid interfaces at rough surfaces, creating contact angles close to 90°. Subsequently, we provide correlations for displacement events as a function of pore-throat geometry. Our findings indicate that having a small throat does not necessarily favor snap-off: the key criterion is the throat radius in relation to the pore radius involved in a displacement event, captured by the aspect ratio.

* Corresponding author at: Institute of GeoEnergy Engineering, Heriot-Watt University, EH14 4AS Edinburgh, UK.
E-mail address: k.singh@hw.ac.uk (K. Singh).

https://doi.org/10.1016/j.jcis.2021.11.109
0021-9797/

1. Introduction

Multiphase flow, including drainage and imbibition, in porous media occurs, for instance, during water infiltration in soils, geo-sequestration of supercritical carbon dioxide (CO_2) in deep saline aquifers or depleted oil and gas fields [1], subsurface non-aqueous phase liquid contaminant transport [2], and oil recovery from reservoir rocks [3]. At low injection rates, typical in earth science applications, capillary forces tend to dominate drainage and imbibition processes. These processes consist of a sequence of several types of fluid displacement event [4–6]. Of particular importance is the amount of non-wetting phase that is trapped during displacement by a wetting phase. This controls, for instance, the efficiency of CO_2 storage, where trapping is desirable, or oil recovery where it limits the amount of production. It is also important in many manufactured fibrous materials, such as surgical masks, where virus-laden water should be trapped, or in fuel cells, where produced water needs to be transported away from the electrodes. Our current understanding is that the non-wetting phase is preferentially trapped in larger regions of the pore space, while the wetting phase favors the filling of narrow regions. In this work we demonstrate that this picture is incomplete and that the non-wetting phase can be retained in small fragments in the corners of a rough surface.

In multiphase flow, drainage is the displacement of a wetting fluid by a non-wetting fluid, and consists of Haines jumps and Roof-snap-off events [7,8]. This process is fairly well understood, in which the fluid displacement follows an invasion percolation pattern controlled by the size of the narrowest regions in the pore space (called throats) between the adjoining widest regions (called pores). By contrast, imbibition, which is controlled by both pore and throat sizes [9], is not straightforward to predict due to the complex interplay and competition of layer and film flow, piston-like displacement and snap-off processes [3,10,11], the latter resulting in the trapping of the non-wetting phase [12–14].

Snap-off is caused by the expulsion of the non-wetting fluid from a throat when wetting layers in throat corners swell and eventually touch, leading to an unstable interface [11]. It is a function of pore-throat geometry and wettability; the latter is described by the fluid–fluid-solid contact angle [3]. Among various geometrical parameters, aspect ratio (the ratio of pore radius to throat radius), angularity or shape and coordination number (the number of throats connected to a pore) have been investigated in previous studies [9, 15-19]. Most quantitative pore-scale studies have been conducted in effectively two-dimensional (2D) micromodels or Hele-Shaw cells. Although these pioneering investigations have helped to explain some of the physical aspects of pore-scale fluid displacement and snap-off processes, the relevance of 2D systems to natural three-dimensional (3D) porous media is poorly understood. Moreover, the effect of surface roughness on interface pinning and fluid displacement has not been fully resolved in natural systems [20,21].

With new developments in X-ray micro-tomography, we can visualize and quantify multiple fluids in the pore space in three dimensions. This technique has been used to study the burst instabilities after Haines jumps [8,22,23], Roof snap-off during drainage [24,25], traditional snap-off during imbibition [11], fluid connectivity [26], ganglion dynamics [27,28], fluid desaturation [29], displacement hysteresis effects [30], interface relaxation dynamics [31], and transition regimes of flow patterns and residual saturation as a function of wettability [23]. Although these displacement processes have been studied extensively, their relationship to 3D geometrical parameters have not been investigated in detail.

A few studies have focused on the relationship of fluid occupancy and residual saturation with pore-throat geometrical parameters. Herring et al. [32] and Andersson et al. [33] have reported a strong correlation of residual saturation of the non-wetting phase with morphological and persistent homology-based aspect ratios and a weaker correlation with the traditional pore-throat aspect ratio. On the other hand, Tanino and Blunt [34] reported a good correlation between residual saturation and the traditional aspect ratio. In their work, an average aspect ratio (ratio of the pore radius to the mean of all bounding throat radii) was used, which does not directly reflect local trapping and pore-filling events. To resolve these conflicting findings, a pore-by-pore analysis of various displacement events is needed. This type of analysis has not been presented in the literature, likely due to the lack of time-resolved tomographic data.

In this study, we have used time-resolved 3D, i.e., four-dimensional (4D), X-ray imaging to investigate the pore-scale dynamics of capillary-controlled imbibition in a carbonate rock sample. We report a previously unidentified snap-off process that occurs in a pore rather than a throat leading to the trapping of the non-wetting fluid in a fraction of a single pore body. We relate this pore-snap-off to roughness-induced interface pinning resulting in increased apparent contact angles locally [35,36]. We also provide new correlations of displacement events with pore-throat geometry, which shows a strong dependence of pore-scale displacement and snap-off processes on the aspect ratio.

2. Materials and methods

2.1. Materials

The experiment was performed on a 3.8 mm diameter and 10 mm long water-wet Ketton limestone rock sample from the Ketton quarry, Rutland, UK, which contains 99.1% calcite with the remaining fraction being quartz [37]. These samples were cleaned with methanol using Soxhlet extraction apparatus for 24 h, followed by drying in a vacuum oven at 100°C for 24 h. A solution of 30 wt% potassium iodide (KI) salt (puriss, 99.5 %, Sigma–Aldrich, UK) in deionized water with a salinity of 1.8 M was used as the aqueous phase, which provided an effective X-ray contrast between brine (wetting phase) and oil (non-wetting phase). Decane (ReagentPlus, $\geqslant$99 %, Sigma–Aldrich, UK) was used as the oil phase.

2.2. Experimental protocol

The details of experimental methodology are presented in Singh et al. [11,38]. Here, we provide a brief description of the experimental protocol. The rock sample was placed on a water-wet porous plate in a Viton sleeve. The assembly was loaded in a Hassler-type flow cell made of carbon fiber that is nearly transparent to X-rays. The end pieces that were fitted to either sides of the sleeve were connected to high-pressure pumps. First, the sample was saturated with brine. The system was then pressurized in steps to 10 MPa with a confining pressure of 11.2 MPa. The oil was then injected from the top at a constant pressure drop of 50 kPa to start drainage. Once there was no further displacement of brine from the sample, the flow was reversed by injecting brine from the base of the sample at a constant pressure drop of 22 kPa, to start imbibition. The capillary number $N_c = v\mu/\sigma$ (where v is the Darcy velocity of the invading fluid, μ is the viscosity of the invading fluid, and σ is the brine-oil interfacial tension) during brine flooding was 1.26×10^{-9}, representing a capillary-dominated flow regime. The sample was imaged continuously during drainage and imbibition using synchrotron X-ray micro-tomography at the Diamond Light

Source, with a voxel size of 3.28 μm and a time-step between consecutive images of 38 s.

2.3. Image processing

The reconstructed tomographic images were filtered using an edge preserving non-local mean filter [39]. The dry filtered image (without fluids) was segmented into two phases (pores and grains) using a seeded watershed algorithm. From the segmented data, we obtain a porosity (i.e., the ratio of the volume of pore space to the total rock volume) of 0.120±0.003 in the complete imaged sample. We then obtained parameters describing pores and throats from the isolated pore space using a pore-throat network approach [40]. This method uses a watershed algorithm on the distance map of the segmented pore space image to identify throats (local constrictions) as boundary surfaces between adjacent pores. Fig. S1 (Supplementary Material) shows the distributions of pore and throat radii as well as pore and throat shape factors obtained from the pore-throat network analysis.

The time-series data containing oil and brine phases were subtracted from the initial image of the rock saturated with brine, to isolate the oil phase, which was then segmented using simple thresholding. The segmented oil was applied as a mask on the pore-throat network to identify the pores and throats that were occupied by oil and brine. By repeating this procedure for each time step (for 285 3D images), we identified the fluid occupancy in each pore and throat at each time step, and subsequently identified snap-offs and pore-filling events by (1) identifying pores/throats where the occupancy changes in a certain time step, and (2) recording the occupancy of all the neighbouring pores and throats in such instances [41]. This analysis guided the calculation of geometrical characteristics of pores and throats involved in pore-filling or snap-off. Note that this analysis on time-resolved images was conducted manually for each time step for quality control. We discarded the events that occurred at the periphery of the sample and at the top and the base of the sample, as the pore-network extraction at these boundaries can result in inaccurate assignment of pore and throat radii.

Brine-oil curvature mapping and capillary pressure. The brine-oil curvature measurements were performed using a method described in Singh et al. [11]. However, the rock phase was dilated by 2 voxels and applied as a mask on the oil curvature maps to remove the curvature values near the three-phase contact line. In this work, we have performed curvature analysis on numerically simulated images that are less distorted near the three-phase contact line, compared to those in 3D images acquired in the experiment. Capillary pressure was then calculated from the measured curvature values using the Young–Laplace equation [11].

3. Results and discussion

3.1. New type of pore-snap-off leading to trapping

Using time-resolved image sequences, we have observed a new type of displacement event leading to the formation of sub-singlet ganglia, occupying less than a pore body. Fig. 1 shows the formation of such a ganglion, in which the oil (non-wetting phase) is displaced from a pore body (Fig. 1A) to the adjacent pore through the oil-filled *throat 3* in the next time step (Fig. 1B). Theoretically, an aspect ratio of more than 2 is favorable for snap-off leading to trapping of the non-wetting phase [3], which is calculated based on 2D geometrical concepts for contact angles close to 0°. The aspect ratio of the pore-throat configuration (the ratio of the radius of the oil-filled pore to the radius of oil-filled *throat 3*) in Fig. 1A is 2.7, therefore a traditional snap-off in *throat 3* leading to trapping of oil in the middle of the pore space was expected. However, neither complete pore-filling nor snap-off (due to brine layer swelling in *throat 3*) occurred; rather the oil-brine interface jumped to the adjacent pore leaving a small fraction of oil which appears to be in a pore corner close to *throat 2*. The oil appears to be stuck to the pore wall crevice, and does not occupy the larger space in the center of the pore as in the case of trapping after a traditional snap-off event [11].

This type of snap-off and trapping has similarities to the fragmentation of a non-wetting phase (oil) observed during desaturation at fast flow rates [43]; however, it cannot be related to the same mechanisms as the flow rate in our study is slower by four orders of magnitude. It may be argued that the interfacial velocity during pore-filling in a slow capillary-dominated flow regime might be extremely high to result in such a fragmentation; however, we hypothesize that the formation of such ganglia is likely to be due to interface pinning at rough edges and corners of the pore space. It may also be that this type of trapping is linked to the traditional snap-off in a separate smaller pore adjacent to the larger pore (refer to Fig. 1 C&D). However, after careful inspection, we have not detected a throat near to the trapped oil. The pore pocket (where trapping occurred, see Fig. 1D) rather appears to be expanding into the larger pore space without any constriction in between. Moreover, if the traditional snap-off had occurred in a throat (if there was a throat), the trapped oil droplet would sit inside the smaller portion of the pore pocket rather than bulging outside into the pore as can be seen in Fig. 1D.

We test our hypothesis of interface pinning induced snap-off by inspecting raw data (gray-scale images). Indeed, the interface pinning at solid surfaces can be observed in Fig. 1C, which results in an advancing contact angle larger than 90° (measured through brine). We further calculated the effective contact angles at various locations on the three-phase contact line (using an automated algorithm [44]), which indicates that locally contact angles close to 90° are seen which we suggest is related to interface pinning (refer to the Supplementary Material - Fig. S2). Interface pinning can occur due to surface roughness [21] or at the patches in the pore space which have different wettability states. The latter is unlikely to occur in our system, because the sample was cleaned before the experiment and was not in contact with any surface active components. We also do not expect pinning due to different mineralogy, as our rock sample consists of 99.1% calcite [37]. We believe that this interface pinning is due to surface roughness that can only be resolved by sub-micrometer scale imaging.

We further tested our hypothesis using direct numerical simulations, which show that pinning of the interface results in pore-snap-off [42]. To mimic the effect of surface roughness, we created a patch on rock surfaces where the trapping of the non-wetting phase occurred (Fig. 1E). The patch was assigned a contact angle of 70° [42], whereas the rest of the surfaces was assigned a contact angle of 45° (which is close to that obtained for a similar brine-oil-rock system at the same pressure and temperature conditions [45]). The patch therefore represents a wettability altered zone caused by roughness-induced pinning. Fig. 1 F-J show snapshots of oil (shown in red) in the pore space at different time steps during brine injection. With increasing brine pressure (or decreasing capillary pressure), brine continues to displace the non-wetting phase from the pore body, without moving the interface at the three-phase contact points (Fig. 1 G-I). The pinning of the interface and further increase in brine pressure results in the development of transverse curvatures (in the opposite direction) at the brine-oil interface (Fig. 1H). The transverse curvatures start to grow (Fig. 1I) and destablize the interface leading to snap-off and trapping (Fig. 1J). Once the oil is disconnected, the interfaces rearrange to attain an equilibrium pressure condition (Fig. 1J). A sensitivity

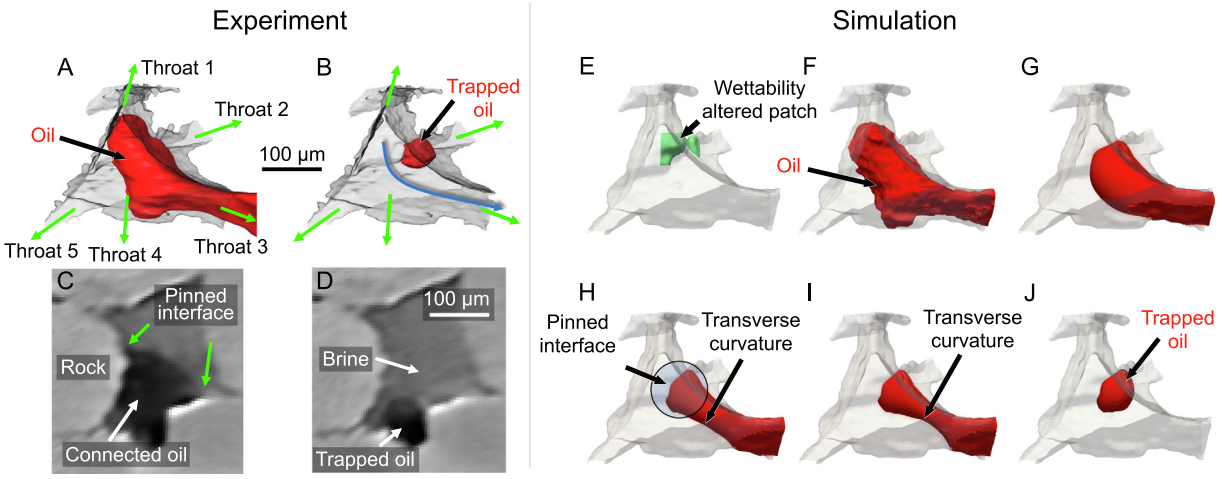

Fig. 1. New type of pore-snap-off leading to the trapping of a non-wetting phase (oil). A-D show the imaging data from the experiment. (A) Oil (non-wetting phase), shown in red, in I_1 configuration at t = 128 min, 34 s. (B) At t = 129 min, 50 s, the oil-brine interface jumps to the adjacent pore, leaving behind a small fraction of oil in the pore space. Here, t represents the time since the start of the imbibition experiment. Brine is shown transparent, while the pore-rock boundary is semi-transparent. (C-D) A two-dimensional slice of the original gray-scale image showing (C) the pinned interface before trapping (at t = 128 min, 34 s), and (D) the trapped non-wetting (oil) phase (at t = 129 min, 50 s). E-J show results from direct numerical simulations [42]. (E) A patch (shown in green) was applied on the rock surface where a contact angle of 70° was assigned, whereas the rest of the rock surface was assigned a contact angle of 45°. A larger contact angle on the patch surface was assigned to mimic a wettability altered zone caused by roughness-induced pinning on the rock surface. (F-J) Snapshots of oil (shown in red) in the pore space at different time steps during brine injection, leading to trapping of the non-wetting phase in the pore corner (J).

analysis of the size and the contact angle of the patch is provided in Shams et al. [42].

The capillary pressures calculated from interfacial curvatures, measured from simulated images (Fig. 1 F-J), are shown in Fig. 2. Initially, there are small fluctuations with a decreasing tend in capillary pressure until the onset of instability marked by dashed-blue line (Fig. 2), which corresponds to fluid configuration in Fig. 1H. The capillary pressure at this point starts to grow until pressure disequilibrium occurs leading to pore-snap-off and trapping. This type of interface instability has similarities to that obtained in traditional snap-off; however, the difference is that the instability in a pore-snap-off occurs inside a pore, as compared to a throat in the case of a traditional snap-off.

We have found 25% of the total snap-off events in our time-series data occurring as pore-snap-off leading to the formation of sub-singlet ganglia. The pore-throat aspect ratio in these pore-snap-off events is in the range of 1.6 to 2.7, which indicates that this type of pore-snap-off is independent of aspect ratio. Moreover, the radii of the pores in which pore-snap-off occurred are in the range 31 μm to 47 μm, whereas the radii of throats in which oil was present before pore-snap-of are in the range 15 μm to 26 μm. Although these pore and throat sizes are in the upper range of the pore size distribution curves (Fig. S1 A-B of the Supplementary Material), further experiments and analysis are needed to investigate statistical correlations with pore and throat sizes.

The findings of this new type of pore-snap-off also have significance, for instance, for mixed-wet systems, and for other types of rock samples, in which different wetting states within a pore can cause interface pinning [46,47], potentially resulting in pore-snap-off leading to trapping.

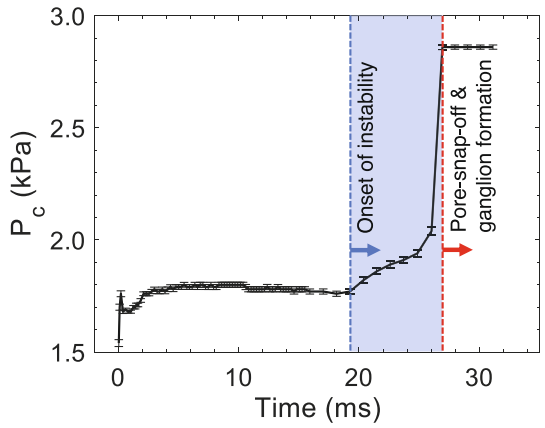

Fig. 2. Capillary pressure calculated from interfacial curvatures, measured from simulated images plotted as a function of time. Here, the dashed-blue shows the onset of instability that leads to pore-snap-off indicted by the dashed-red line. The error bars in the capillary pressure are standard error in the mean with 95% confidence intervals.

3.2. Fluid displacement correlations with pore-throat geometry

Fig. 3 C-I show pore-scale events (*1* to *9*) in a sequence according to the time they occurred in a small subset of 220 × 290 × 190 voxels. The non-wetting phase (red) from the time-resolved segmented data is superimposed on a pore-throat network extracted from the pore space (Fig. 3 A-B), to characterize various pore-throat geometrical properties involved in fluid displacement events. A video of the image sequence of fluid displacement superimposed on a pore-throat network in this subset is available online in Ref [48].

Two important geometrical parameters, i.e., aspect ratio (the ratio of pore radius to throat radius involved in a displacement event) and the shape factor ($G = R^2/(4A)$, where R is the radius of the inscribed sphere, and A is the cross-sectional area of the pore or throat [40,49]), are studied in this analysis. We find that the aspect ratio for pore-filling events (i.e., brine displacing oil in pores) is in the range of 1.2 to 1.6 (*events 1*, *2*, *3*, *4*, *5*, *7* and *8*), except for *event 9* that has a value of 2.1. Note that *event 8* and *event 9* occurred during the same time step after the snap-off *event 6*. The interfacial jump after *event 6* could have created pressure fluctuations in the adjacent pores, which could have led to pore-filling for an unfavorable aspect ratio in *event 9* [28]. The aspect ratio for the snap-off event *6* is 3, which is substantially larger than that for pore-filling events, therefore, resulting in unfavorable con-

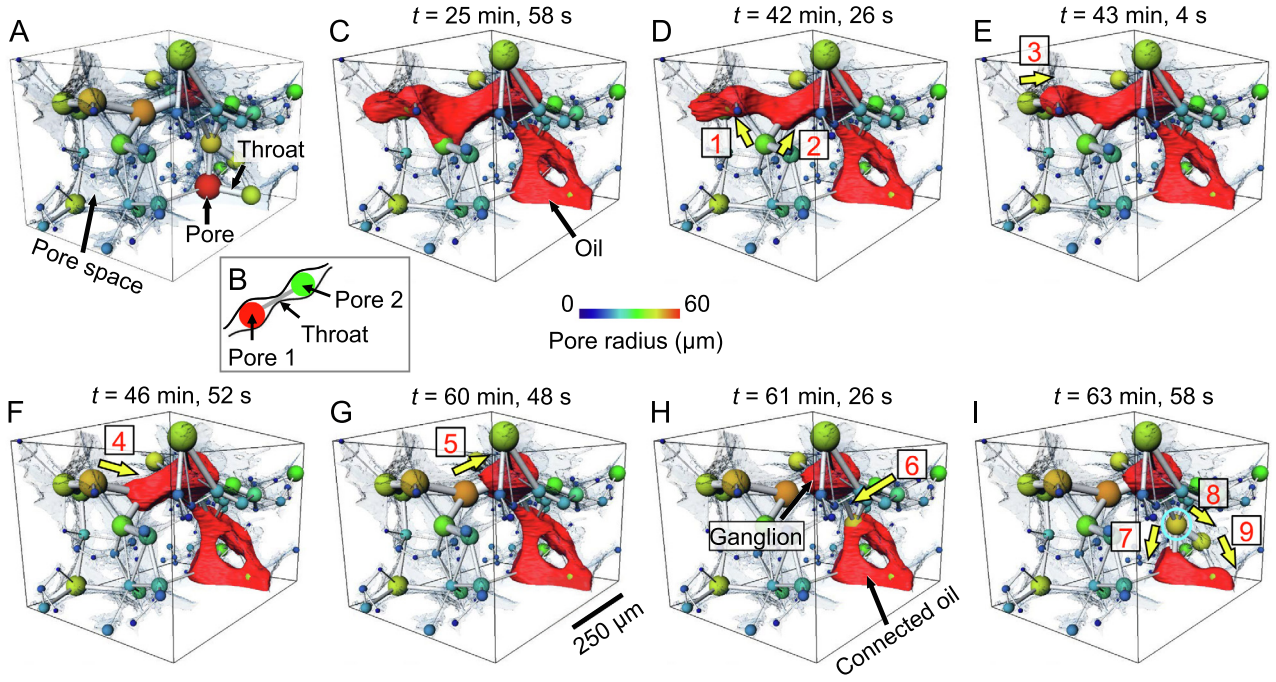

Fig. 3. Pore-filling and snap-off events during imbibition in a carbonate rock. Here, the analysis is performed on a small subset of 220 × 290 × 190 voxels, where the size of each voxel is 3.28 μm. (A) A pore-throat network generated from the pore space of the segmented image was used to analyze the characteristics of filling events observed in the experiment. The pores are the largest inscribed spheres in the separated pore space, which are colored according to size. Throats, represented by gray rods, are the narrowest constriction along the medial axis connecting two adjacent pores. (B) A sketch of pore and throat extraction. The pores are represented as maximum radius circles (spheres in 3D) that fit into the pores space, such as Pore 1 and Pore 2. Throats are represented as tubes connecting two pores. The tube has the same radius as the constriction separating the pores. (C) The oil phase from time-resolved tomography (at t = 25 min, 58 s) was superimposed on the pore-throat network shown in (A). (C-I) Various time steps showing different displacement events (pore-filling and snap-off) during imbibition. Here, t represents the time since the start of the imbibition experiment. Brine and rock are shown transparent and semi-transparent respectively for effective visualization. A time-lapse video of these events is available in Ref [48].

ditions for pore-filling. This finding is consistent with previous theoretical predictions on 2D geometries, which suggest that a large aspect ratio is favorable for snap-off [3].

The shape factor of throats involved in pore-filling events is in the range of 0.029 to 0.049, whereas for the snap-off *event 6*, the shape factor is 0.026. Smaller throat shape factors are favorable for snap-off, since this represents throats with a large surface area and smaller corner angles, which are likely to have more corners in which wetting layers can reside and swell with time (with decreasing capillary pressure or increasing brine pressure) leading to snap-off.

We further extend this analysis to the complete scanned image (1189 × 1163 × 1000 voxels) of the whole time-series (285 3D images). To simplify this analysis, we first divide pore-scale displacement events into I_n event types (Fig. 4 A-C), originally proposed by Lenormand and co-workers [13,50], where n indicates the number of throats filled by the non-wetting phase (oil) connected to a pore in question; these throats are emptied by brine between two consecutive images. The majority of fluid displacements are found to be I_1 (68%) and I_2 (22%) events (Fig. 4D), which occurred more frequently than snap-off. Only a few I_3 events (approximately 2%) are observed in the data analyzed. This observation is expected as a higher brine pressure (or lower capillary pressure that can be calculated using a simple geometrical analysis) is needed to displace oil in I_2 and I_3 events compared to I_1 events, thereby making I_1 the predominant pore-filling process during imbibition [51].

Fig. 4G shows the distribution of aspect ratios for various I_1 pore-filling events (blue bars) and threshold aspect ratios for snap-off events (dashed lines). The competition between a pore-filling I_1 and a snap-off event is illustrated in Fig. 4E, in which the non-wetting phase can experience either a snap-off event in the throat or a pore-filling event from Pore 2 to Pore 1 (in which Pore 2 is emptied). Most of such I_1 pore-filling events occurred for an aspect ratio less than 2 (Fig. 4G), with an average value of 1.4±0.3 (mean±SD). The smallest (threshold) value of the aspect ratio for which we observe a snap-off followed by trapping is 2.15 (dashed gray line in Fig. 4G). This finding is in agreement with the previous subset analysis in Fig. 3. We also observed a pore-filling I_1 event that occurred for an unfavorable aspect ratio of 2.49. This pore-filling event was observed immediately after a snap-off event in the adjacent pore, and may be related to inertial effects as described for *event 9* in Fig. 3I and reported in a previous study [28].

Similarly, the snap-off in a throat between two pores containing connected oil (Fig. 4F) shows a good correlation with aspect ratio. In this case, the non-wetting phase does not experience entrapment after snap-off. A threshold value of 2.03 is found for snap-off without trapping (dashed black line in Fig. 4G). In this analysis, the maximum aspect ratio of a throat undergoing snap-off considering its two neighboring pores was considered.

These observed values of the threshold aspect ratio for snap-off are consistent with the theoretical value of 2 (obtained from 2D geometrical analysis) for contact angles close to 0° (for strongly wetting or hydrophilic conditions) [3]. However, our results are different from those obtained in previous 2D experimental studies, which report that the minimum (threshold) aspect ratio for which snap-off events occur increases from 1.50 to 1.75 for an increase in contact angle from 0° to 55° [9,52]. The threshold aspect ratio becomes infinite for contact angles larger than 70°, and snap-off cannot occur in this case. The difference in the threshold aspect ratios from those found in our analysis is likely to be due to 2D geometry of the model experimental systems used in the previous studies.

The average value of the aspect ratios for I_2 and I_3 events (Fig. 4G, orange bars) is 1.8±0.5 (mean±SD). 28% of I_2 and I_3

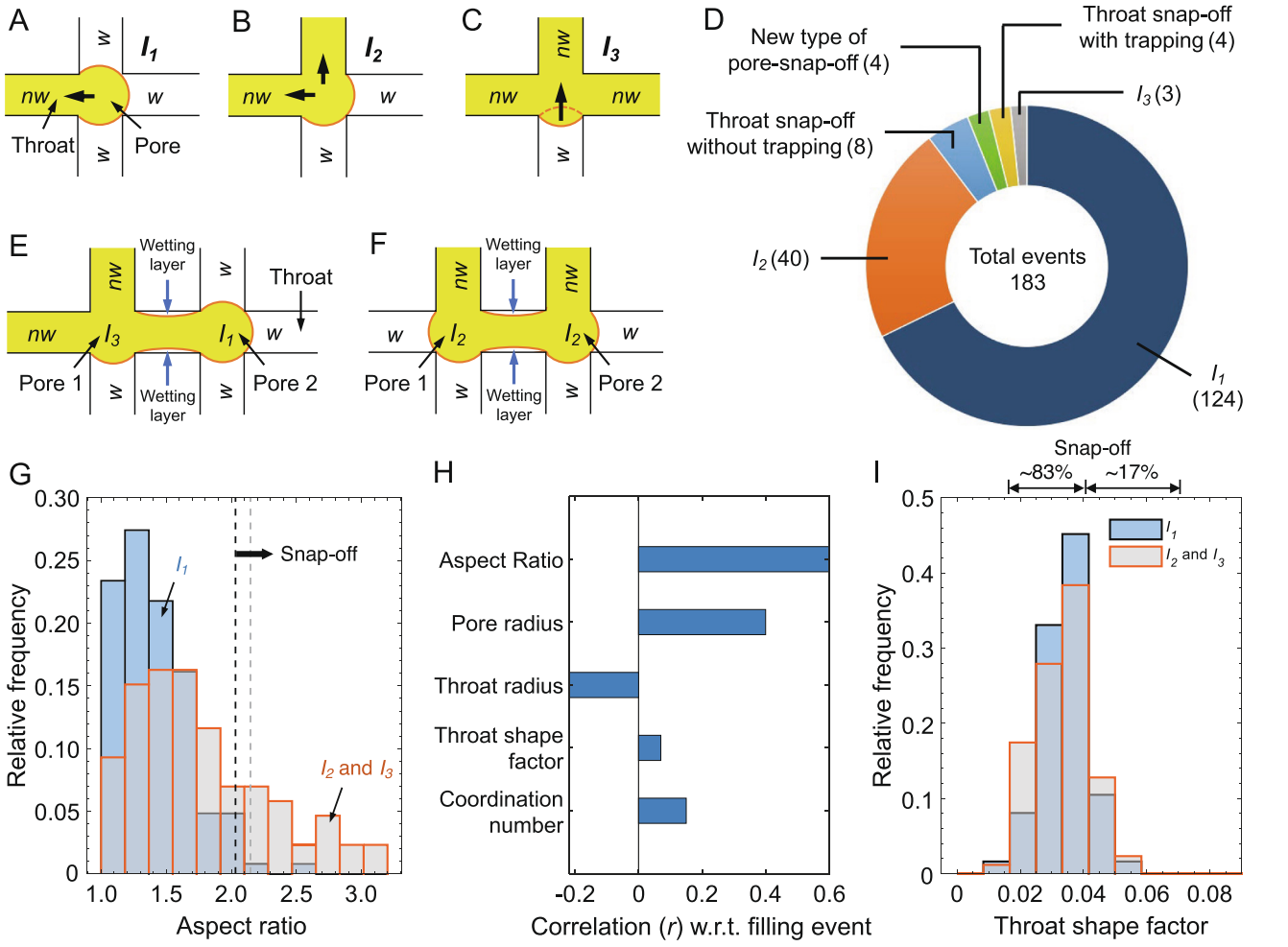

Fig. 4. I_n fluid configurations and correlations with pore-throat geometry. (A-C) I_n configuration and pore-filling description in a square lattice with a co-ordination number of four (after Lenormand and co-workers [13,50]). A displacement event is called I_1 if one of the throats is initially filled with a non-wetting fluid (A). Similarly, I_2 and I_3 pore-filling events are defined when two and three throats are initially filled with the non-wetting fluid respectively (B and C). *w* and *nw* refer to wetting and non-wetting fluids respectively. Large black arrows show the direction of fluid displacement. (D) Frequency of different types of events observed during imbibition. This analysis has been performed on 285 time-resolved 3D images of 1189 × 1163 × 1000 voxels. (E) An I_1 configuration experiencing either a pore-filling event from Pore 2 to Pore 1 or wetting layer swelling in the throat leading to snap-off and trapping in Pore 2. (F) Wetting layer swelling between two connected pores with I_2 configurations leading to snap-off in the throat. In this case, the non-wetting fluid after snap-off stays connected. (G) Aspect ratio distributions for I_1, I_2 and I_3 events. Dashed gray and black lines show minimum (threshold) values of aspect ratios obtained for snap-off resulting in oil trapping (for I_1 configurations) and snap-off without trapping between connected oil in two pores respectively. (H) Correlation (Pearson's *r*) with respect to filling event showing relationship between displacement events (snap-off/I_n) and pore-throat geometry. (I) Throat shape factor distribution for I_1, I_2 and I_3 events. Throat shape factors for snap-off events are overlain on the data along the top *x*-axis.

pore-filling events occurred for an aspect ratio larger than 2. In these events, it is likely that a snap-off occurred in one or more throats leading to a piston-like displacement in other throats. The time resolution of tomography is not sufficient to confirm this hypothesis. This would need further investigation by conducting faster tomography or direct numerical simulations.

To investigate how well geometrical characteristics explain the observed filling types, we have calculated the correlations between pore-throat geometric parameters and displacement events (snap-off, I_n), as shown in Fig. 4H. The correlation of two variables was obtained by calculating the Pearson correlation coefficient (Pearson's *r*).

$$r = \frac{\sum_{i=1}^{n}(x_i - \bar{x})(y_i - \bar{y})}{\sqrt{\sum_{i=1}^{n}(x_i - \bar{x})^2}\sqrt{\sum_{i=1}^{n}(y_i - \bar{y})^2}} \quad (1)$$

where $\bar{x}$ and $\bar{y}$ are the mean values of variables *x* and *y* respectively. x_i and y_i are individual data points of variables *x* and *y* respectively. We have used x_i as an indicator function which shows whether it is an I_n event (value = 0) or a snap-off (value = 1). The second variable y_i is the pore-throat parameter studied (e.g., aspect ratio, pore radius, throat radius, throat shape factor and pore coordination number). The values of Pearson's *r* can range from −1 to + 1, where values close to −1 and + 1 indicate strong correlations between the event type and geometric parameter in question, whereas a value of 0 shows no correlation. The analysis presented in Fig. 4H shows that the aspect ratio is strongly correlated to the occurrence of snap-off or I_n events, with Pearson's *r* in the range 0.6 and low *p*-values (the probability of no correlation; the values are reported in Table S1 in the Supplementary Material). This analysis is consistent with the analysis presented in Fig. 4G. The observation of a strong correlation of pore-scale events with the aspect ratio is important. For instance, the implementation of these correlations in pore-network models is likely to improve the accuracy of predictions. Pore-network models

are frequently used for the prediction of multiphase flow in 3D porous media [14,41,53], due to their fast run time and the possibility of upscaling them to larger domains, which is a limitations of more accurate direct numerical simulations. However, further time-resolved experiments on different rock types and wettability are required to generalise our findings and implement them in pore-network simulations.

Pore radius and snap-off/I_n show a good correlation (Fig. 4H), indicating that pore filling is suppressed when the pore involved is large; however, throat radius shows a poor correlation with high p-values (Supplementary Material). This observation indicates that just having a small throat does not necessarily favor snap-off over pore-filling: the key criterion is the throat radius in relation to the pore, which is captured by the aspect ratio. The coordination number analysis for snap-off/I_n events shows a poor correlation, which could be due to misidentification of snap-off followed by I_1 events as I_2 events (due to the limited time resolution of the measurements).

The throat shape factor shows weaker correlations (Fig. 4H) with significantly higher probability of the null hypothesis (no relationship), refer to Table S1, Supplementary Material. This observation is consistent with the findings reported in Fig. 4I. Although a majority of snap-off events occurred in throats with lower throat shape factors (Fig. 4I), the range of these values overlaps with the distribution of throat shape factors for I_1, I_2 and I_3 events. This unexpected result could be due to a limited voxel count in throats (due to image resolution) which does not allow for the accurate estimation of shape factors. Additional experiments using sub-micrometer resolution 4D imaging are needed to provide further details.

3.3. Unexpected I_2 pore-filling event

We have observed an I_2 pore-filling event that occurred for unfavorable aspect ratios. Fig. 5A shows this I_2 fluid configuration where two throats connected to a pore are occupied by the non-wetting phase (oil). In the next time step, the non-wetting phase is displaced to the adjacent pores through the throats (Fig. 5B). The aspect ratios involved in the displacement *event 1* and *event 2* are 3.3 and 4.4 respectively, which are favorable for snap-off and oil trapping; however, the oil migrates to the adjacent pores without being trapped. It is possible that a snap-off event occurred in one of the throats, resulting in a subsequent I_1 event through the other throat potentially due to inertial effects caused by the snap-off. We cannot exclude that this type of displacement event is more important in other pore geometries without understanding what causes it; therefore further research is needed.

4. Conclusions

Using fast 4D synchrotron X-ray micro-tomography, we have identified a new type of pore-snap-off that occurs in pores leading to non-wetting phase trapping in a fraction of a pore body. This contrasts with traditional snap-off that occurs in throats leading to trapping of the non-wetting phase in pore centers [12,54]. We relate the new type of pore-snap-off to interface pinning at rough pore surfaces, which results in an advancing contact angle close to 90° during displacement in a water-wet (hydrophilic) system. This type of pore-snap-off could also occur in mixed-wet systems, where interface pinning can happen at different wettability sections within a pore [45,55].

Our analysis also provides important insights into various displacement events such as I_n pore-filling, snap-off and trapping during imbibition. By extracting a pore-throat network and superimposing it on the oil phase in consecutive time-series images, we have analyzed conditions that are favorable for each event type. The Pearson correlation coefficient and the null hypothesis probability showed that the aspect ratio has a strong influence on whether a snap-off or a pore-filling event occurred. Aspect ratios less than 2.15 (threshold value) were found to be favorable for I_1 pore-filling, except for 3% of I_1 events that occurred for more than this threshold value. This threshold value is significantly larger than the values 1.50 to 1.75 reported in the literature [9,52], which were obtained using 2D experimental studies. The difference in the threshold aspect ratios is likely to be due to 2D geometry of systems used in the previous studies, which suggests that model 2D systems cannot always reproduce quantitative information of natural 3D systems or it would at least require some scaling parameters.

Furthermore, our results show that 28% of I_2 and I_3 pore-filling events occurred for an aspect ratio larger than 2. Firstly, these unfavorable pore-filling events may be related to inertial effects, especially after a snap-off event in an adjacent throat; however, further research is needed to support this hypothesis. Secondly, this unfavorable pore-filling may be due to misidentification of snap-off followed by I_1 and I_2 as I_2 and I_3 events respectively, which may be due to limited time resolution. We have also identified an unexpected I_2 pore-filling event for high aspect ratios that were favorable for snap-off; however, the time resolution is not sufficient to investigate it further. Future work can focus on using

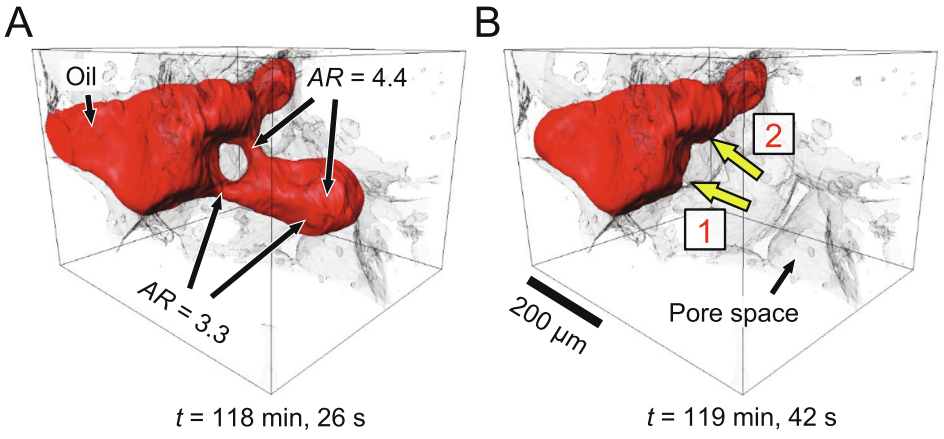

Fig. 5. Unexpected I_2 pore-filling event. (A) Oil (non-wetting phase) in I_2 configuration at t = 118 min, 26 s. (B) The oil-brine interface is displaced to adjacent pores at t = 119 min, 42 s. Here, *AR* represents the aspect ratio, and t represents the time since the start of the imbibition experiment.

faster synchrotron imaging [56] or the visualization of flow in 3D printed micromodels [57] along with direct numerical simulations [42,58–60] to investigate these processes in detail.

Overall, the analysis and correlations provided in this study improve our general understanding of the physics of fluid flow in water-wet porous media, and consequently of pore-scale models of fluid displacement processes. Specifically, this new type of trapping in pores needs to be incorporated into existing multiphase flow models. Further experiments and similar analysis on porous media with altered wettability, or on other types of porous media, e.g., sand packs, sandstones and more complex carbonate rocks, are needed to extend the generality of our approach. With a complete understanding of pore-scale processes, we will be able to design materials and processes that either maximize or minimize the amount of trapping, dependent on application.

Data availability statement

The raw and processed tomographic datasets have been uploaded on a public repository (BGS), the details of which are provided in Ref [61].

Author contributions

Kamaljit Singh: Conceptualization, Methodology, Software, Formal analysis, Investigation, Data Curation, Writing, Visualization, Project administration. **Tom Bultreys**: Methodology, Software, Formal analysis, Investigation, Writing. **Ali Q. Raeini**: Methodology, Software, Formal analysis, Investigation, Writing. **Mosayeb Shams**: Methodology, Software, Formal analysis, Investigation, Writing. **Martin J. Blunt**: Conceptualization, Methodology, Formal analysis, Investigation, Data Curation, Writing, Supervision, Project administration, Funding acquisition.

Declaration of competing interest

The authors declare that they have no known competing financial interests or personal relationships that could have appeared to influence the work reported in this paper.

Acknowledgements

We gratefully acknowledge funding from the Qatar Carbonates and Carbon Storage Research Centre (QCCSRC), provided jointly by Qatar Petroleum, Shell, and Qatar Science and Technology Park. We thank Hannah Menke, Matthew Andrew, Branko Bijeljic, Tarik Saif, Norman Nicholls, Vincenzo Cunsolo, Joan Vila-Comamala and Christoph Rau for help in imaging. We thank the Diamond Light Source for access to beamline I13 (MT11587). T.B. is a postdoctoral fellow of the Research Foundation-Flanders (FWO) and acknowledges its support under grant 12X0919N. A.Q.R thanks Total and Wintershall DEA for their financial support. M.S. acknowledges the support of the Natural Environment Research Council via grant NE/N016173/1. We thank Steffen Berg for valuable comments and discussion.

Appendix A. Supplementary material

Supplementary data associated with this article can be found, in the online version, at https://doi.org/10.1016/j.jcis.2021.11.109.

References

[1] S. Krevor, M.J. Blunt, S.M. Benson, C.H. Pentland, C. Reynolds, A. Al-Menhali, B. Niu, Capillary trapping for geologic carbon dioxide storage - From pore scale physics to field scale implications, Int. J. Greenhouse Gas Control 40 (2015) 221–237.
[2] T. Pak, L.F.L. Luz, T. Tosco, G.S.R. Costa, R.P.R. Rangel, N.L. Archilha, Pore-scale investigation of the use of reactive nanoparticles for in situ remediation of contaminated groundwater source, in: Proc. Nat. Acad. Sci., 2020.
[3] M.J. Blunt, Multiphase Flow in Permeable Media: A Pore-Scale Perspective, Cambridge University Press, 2017.
[4] S. Pavuluri, J. Maes, J. Yang, M. Regaieg, A. Moncorge, F. Doster, Towards pore network modelling of spontaneous imbibition: Contact angle dependent invasion patterns and the occurrence of dynamic capillary barriers, Computational Geo-sciences. (2019).
[5] I. Zacharoudiou, E.M. Chapman, E.S. Boek, J.P. Crawshaw, Pore-filling events in single junction micro-models with corresponding lattice Boltzmann simulations, J. Fluid Mech. 824 (2017) 550–573.
[6] R. Hu, J. Wan, Z. Yang, Y.-F. Chen, T. Tokunaga, Wettability and flow rate impacts on immiscible displacement: A theoretical model, Geophys. Res. Lett. 45 (2018) 3077–3086.
[7] W.B. Haines, Studies in the physical properties of soil. V. The hysteresis effect in capillary properties, and the modes of moisture distribution associated therewith, The Journal of Agricultural Science 20 (1930) 97–116.
[8] S. Berg, H. Ott, S.A. Klapp, A. Schwing, R. Neiteler, N. Brussee, A. Makurat, L. Leu, F. Enzmann, J.-O. Schwarz, M. Kersten, S. Irvine, M. Stampanoni, Real-time 3D imaging of Haines jumps in porous media flow, Proc. Nat. Acad. Sci. 110 (2013) 3755–3759.
[9] L. Yu, N.C. Wardlaw, Mechanisms of nonwetting phase trapping during imbibition at slow rates, J. Colloid Interface Sci. 109 (1986) 473–486.
[10] B. Zhao, C.W. MacMinn, R. Juanes, Wettability control on multiphase flow in patterned microfluidics, Proc. Nat. Acad. Sci. 113 (2016) 10251–10256.
[11] K. Singh, H. Menke, M. Andrew, Q. Lin, C. Rau, M.J. Blunt, B. Bijeljic, Dynamics of snap-off and pore-filling events during two-phase fluid flow in permeable media, Scientific Reports 7 (2017) 5192.
[12] J. Pickell, B. Swanson, W. Hickman, Application of air-mercury and oil-air capillary pressure data in the study of pore structure and fluid distribution, Soc. Petrol. Eng. J. 6 (1966) 55–61.
[13] R. Lenormand, C. Zarcone, Role of roughness and edges during imbibition in square capillaries, In SPE Annual Technical Conference and Exhibition (1984).
[14] L. Ruspini, R. Farokhpoor, P. Øren, Pore-scale modeling of capillary trapping in water-wet porous media: A new cooperative pore-body filling model, Adv. Water Resour. 108 (2017) 1–14.
[15] V.H. Nguyen, A.P. Sheppard, M.A. Knackstedt, W.V. Pinczewski, The effect of displacement rate on imbibition relative permeability and residual saturation, J. Petrol. Sci. Eng. 52 (2006) 54–70.
[16] I. Chatzis, N.R. Morrow, Magnitude and detailed structure of residual oil saturation, Society of Petroleum Engineers Journal 23 (1983) 311–326.
[17] L. He, Z. Luo, B. Bai, Breakup of pancake droplets flowing through a microfluidic constriction, Chem. Eng. Sci. 220 (2020) 115649.
[18] A. Kovscek, C. Radke, Gas bubble snap-off under pressure-driven flow in constricted noncircular capillaries, Colloids Surf., A 111 (1996) 55–76.
[19] B. Legait, Laminar flow of two phases through a capillary tube with variable square cross-section, in: Journal of colloid and interface science 96, 1983.
[20] B. Zulfiqar, H. Vogel, Y. Ding, S. Golmohammadi, M. Küchler, D. Reuter, H. Geistlinger, The Impact of Wettability and Surface Roughness on Fluid Displacement and Capillary Trapping in 2-D and 3-D Porous Media: 2. Combined Effect of Wettability, Surface Roughness, and Pore Space Structure on Trapping Efficiency in Sand Packs and Micromodels, Water Resour. Res. 56 (2020). e2020WR027965.
[21] F.-C. Yang, X.-P. Chen, P. Yue, Surface roughness effects on contact line motion with small capillary number, Phys. Fluids 30 (2018) 012106.
[22] T. Bultreys, M. Boone, M. Boone, T. De Schryver, B. Masschaele, D. Van Loo, L. Van Hoorebeke, V. Cnudde, Real-time visualization of Haines jumps in sandstone with laboratory-based microcomputed tomography, Water Resour. Res. 51 (2015) 8668–8676.
[23] K. Singh, H. Scholl, M. Brinkmann, M.D. Michiel, M. Scheel, S. Herminghaus, R. Seemann, The role of local instabilities in fluid invasion into permeable media, Scientific Reports 7 (2017) 444.
[24] M. Andrew, H. Menke, M.J. Blunt, B. Bijeljic, The imaging of dynamic multiphase fluid flow using synchrotron-based X-ray microtomography at reservoir conditions, Transp. Porous Media 110 (2015) 1–24.
[25] K. Singh, M. Jung, M. Brinkmann, R. Seemann, Capillary-dominated fluid displacement in porous media, Annu. Rev. Fluid Mech. 51 (2019) 429–449.
[26] C.A. Reynolds, H. Menke, M. Andrew, M.J. Blunt, S. Krevor, Dynamic fluid connectivity during steady-state multiphase flow in a sandstone, Proc. Nat. Acad. Sci. 114 (2017) 8187–8192.
[27] S. Berg, R.T. Armstrong, A. Georgiadis, H. Ott, A. Schwing, R. Neiteler, N. Brussee, A. Makurat, M. Rucker, L. Leu, M. Wolf, F. Khan, F. Enzmann, M. Kersten, Onset of oil mobilization and nonwetting-Phase cluster-size distribution, Petro-physics 56 (2015) 15–22.
[28] M. Rucker, S. Berg, R.T. Armstrong, A. Georgiadis, H. Ott, A. Schwing, R. Neiteler, N. Brussee, A. Makurat, L. Leu, M. Wolf, F. Khan, F. Enzmann, M. Kersten, From connected pathway flow to ganglion dynamics, Geophys. Res. Lett. 42 (2015) 3888–3894.
[29] R.T. Armstrong, A. Georgiadis, H. Ott, D. Klemin, S. Berg, Critical capillary number: Desaturation studied with fast X-ray computed microtomography, Geophys. Res. Lett. 41 (2014) 55–60.

[30] S. Schlüter, S. Berg, M. Rücker, R.T. Armstrong, H.-J. Vogel, R. Hilfer, D. Wildenschild, Pore-scale displacement mechanisms as a source of hysteresis for two-phase flow in porous media, Water Resour. Res. 52 (2016) 2194–2205.
[31] S. Schlüter, S. Berg, T. Li, H.-J. Vogel, D. Wildenschild, Time scales of relaxation dynamics during transient conditions in two-phase flow, Water Resour. Res. 53 (2017) 4709–4724.
[32] A.L. Herring, V. Robins, A.P. Sheppard, Topological persistence for relating microstructure and capillary fluid trapping in sandstones, Water Resour. Res. 55 (2019) 555–573.
[33] L. Andersson, A. Herring, S. Schlüter, D. Wildenschild, Defining a novel pore-body to pore-throat "Morphological Aspect Ratio" that scales with residual non-wetting phase capillary trapping in porous media, Adv. Water Resour. 122 (2018) 251–262.
[34] Y. Tanino, M.J. Blunt, Capillary trapping in sandstones and carbonates: Dependence on pore structure, Water Resour. Res. 48 (2012).
[35] S. Herminghaus, Roughness-induced non-wetting, Europhysics Letters (EPL) 52 (2000) 165–170.
[36] M. Nosonovsky, B. Bhushan, Roughness-induced superhydrophobicity: a way to design non-adhesive surfaces, J. Phys.: Condens. Matter 20 (2008) 225009.
[37] M. Andrew, B. Bijeljic, M.J. Blunt, Pore-scale imaging of trapped supercritical carbon dioxide in sandstones and carbonates, Int. J. Greenhouse Gas Control 22 (2014) 1–14.
[38] K. Singh, H. Menke, M. Andrew, C. Rau, B. Bijeljic, M.J. Blunt, Time-resolved synchrotron X-ray micro-tomography datasets of drainage and imbibition in carbonate rocks, Scientific Data 5 (2018) 180265.
[39] A. Buades, B. Coll, J. Morel, Nonlocal image and Movie denoising, Int. J. Comput. Vision 16 (2008) 123–139.
[40] A.Q. Raeini, B. Bijeljic, M.J. Blunt, Generalized network modeling: Network extraction as a coarse-scale discretization of the void space of porous media, Phys. Rev. E 96 (2017) 013312.
[41] T. Bulreys, K. Singh, A.Q. Raeini, L.C Ruspini, P.E. Oren, S. Berg, M. Rücker, B. Bijeljic, M.J. Blunt, Verifying pore network models of imbibition in rocks using time-resolved synchrotron imaging, Water Resources Research 56 (2020) e2019WR026587.
[42] M. Shams, K. Singh, B. Bijeljic, M.J. Blunt, Direct numerical simulation of pore-scale trapping events during capillary-dominated two-phase flow in porous media, Transp. Porous Media 138 (2021) 443–458.
[43] P. Pak, I.B. Butler, S. Geiger, M.I.J. van Dijke, K.S. Sorbie, Droplet fragmentation: 3D imaging of a previously unidentified pore-scale process during multiphase flow in porous media, Proc. Nat. Acad. Sci. 112 (2015) 1947–1952.
[44] A. AlRatrout, A.Q. Raeini, B. Bijeljic, M.J. Blunt, Automatic measurement of contact angle in pore-space images, Adv. Water Resour. 109 (2017) 158–169.
[45] K. Singh, B. Bijeljic, M.J. Blunt, Imaging of oil layers, curvature and contact angle in a mixed-wet and a water-wet carbonate rock, Water Resour. Res. 52 (2016) 1716–1728.
[46] J. Schmatz, J.L. Urai, S. Berg, H. Ott, Nanoscale imaging of pore-scale fluid-fluid-solid contacts in sandstone, Geophys. Res. Lett. 42 (2015) 2189–2195.
[47] A. AlRatrout, M.J. Blunt, B. Bijeljic, Wettability in complex porous materials, the mixed-wet state, and its relationship to surface roughness, Proc. Nat. Acad. Sci. 115 (2018) 8901–8906.
[48] K. Singh, Pore-filling and snap-off events superimposed on a pore-throat network extracted from the segmented pore space, Figshare (2019), https://doi.org/10.6084/m9.figshare.9034367.v1.
[49] T. Bultreys, Q. Lin, Y. Gao, A.Q. Raeini, A. AlRatrout, B. Bijeljic, M.J. Blunt, Validation of model predictions of pore-scale fluid distributions during two-phase flow, Phys. Rev. E 97 (2018) 053104.
[50] R. Lenormand, C. Zarcone, A. Sarr, Mechanisms of the displacement of one fluid by another in a network of capillary ducts, J. Fluid Mech. 135 (1983) 337–353.
[51] P.H. Valvatne, M.J. Blunt, Predictive pore-scale modeling of two-phase flow in mixed wet media, Water Resour. Res. 40 (2004).
[52] L. Yu, N.C. Wardlaw, The influence of wettability and critical pore-throat size ratio on snap–off, J. Colloid Interface Sci. 109 (1986) 461–472.
[53] A.Q. Raeini, J. Yang, I. Bondino, T. Bultreys, M.J. Blunt, B. Bijeljic, Validating the generalized pore network model using micro-CT images of two-phase flow, Transp. Porous Media (2019).
[54] K.K. Mohanty, H.T. Davis, L.E. Scriven, Physics of oil entrapment in water-wet rock, SPE Reservoir Engineering 2 (1987) 113–128.
[55] A. Scanziani, Q. Lin, A. Alhosani, M.J. Blunt, B. Bijeljic, Dynamics of fluid displacement in mixed-wet porous media, Proceedings of the Royal Society A: Mathematical, Physical and Engineering Sciences 476 (2020) 20200040.
[56] R. Mokso, C.M. Schleputz, G. Theidel, H. Billich, E. Schmid, T. Celcer, G. Mikuljan, L. Sala, F. Marone, N. Schlumpf, M. Stampanoni, GigaFRoST: the gigabit fast readout system for tomography, Journal of Synchrotron Radiation 24 (2017) 1250–1259.
[57] S. Ishutov, T.D. Jobe, S. Zhang, M. Gonzalez, S.M. Agar, F.J. Hasiuk, F. Watson, S. Geiger, E. Mackay, R. Chalaturnyk, Three-dimensional printing for geoscience: Fundamental research, education, and applications for the petroleum industry, AAPG Bulletin 102 (2018) 1–26.
[58] M. Shams, A.Q. Raeini, M.J. Blunt, B. Bijeljic, A numerical model of two-phase flow at the micro-scale using the volume-of-fluid method, J. Comput. Phys. 357 (2018) 159–182.
[59] J. Maes, C. Soulaine, A new compressive scheme to simulate species transfer across fluid interfaces using the Volume-Of-Fluid method, Chem. Eng. Sci. 190 (2018) 405–418.
[60] A.Q. Raeini, M.J. Blunt, B. Bijeljic, Modelling two-phase flow in porous media at the pore scale using the volume-of-fluid method, J. Comput. Phys. 231 (2012) 5653–5668.
[61] K. Singh, M.J. Blunt, High-resolution time-resolved synchrotron X-ray micro-tomography datasets of drainage and imbibition in carbonate rocks at reservoir pressure conditions, British Geological Survey (2018). https://doi.org/10.5285/3aa44060-d4fd-453f-9e5b-7d885ad5089f.